γ decay from states at low excitation energy in the neutron-deficient isotope, ^{200}Rn, identified by correlated radioactive decay

R. B. E. Taylor, S. J. Freeman, J. L. Durell, M. J. Leddy, and A. G. Smith
Schuster Laboratory, University of Manchester, Manchester M13 9PL, United Kingdom

D. J. Blumenthal,* M. P. Carpenter, C. N. Davids, C. J. Lister, R. V. F. Janssens, and D. Seweryniak
Argonne National Laboratory, Argonne, Illinois 60439

(Received 23 August 1996)

The low-lying level structure of the neutron-deficient isotope ^{200}Rn has been studied using the ^{176}Hf(^{28}Si,$4n$) reaction at a beam energy of 142 MeV. Evaporation residues were selected using an in-flight recoil mass separator, the Argonne Fragment Mass Analyzer, and implanted in a double-sided silicon strip detector. Prompt γ rays in ^{200}Rn were observed at the target position using the AYEBALL array of 19 Compton-suppressed germanium detectors, and were identified by the subsequent radioactive decay of associated recoiling ions in the strip detector. Isotopic assignments of the nuclei produced were made on the basis of the mass-to-charge ratio of the recoiling ion and the energy and half-life of its α decay. Previous results concerning transitions in ^{202}Rn were confirmed. The level scheme deduced for ^{200}Rn, compared with those of heavier radon isotopes, is not consistent with the onset of deformation predicted by theoretical calculations. The estimated production cross section for ^{200}Rn in this reaction was 5 μb. [S0556-2813(96)04812-1]

PACS number(s): 27.80.+w, 23.20.Lv, 23.60.+e, 25.70.Gh

I. INTRODUCTION

With the addition of valence protons and neutrons outside of the doubly magic ^{208}Pb core, polarizing effects are evident with the onset of permanently deformed ground-state shapes in actinide isotopes with $N>126$ and $Z>82$. In contrast, the structural consequences associated with the addition of valence particles, in combination with valence holes, are not established experimentally. In the region of isotopes with $N<126$ and $Z>82$, there have been many theoretical calculations [1–5] which indicate the possibility of an extended region of deformed nuclei far from stability.

Nuclei far from stability in the $N<126$ and $Z>82$ region have not been extensively studied in experiments sensitive to nuclear deformation. Laser spectroscopy measurements show some evidence for a softening of spherical shape, but there is no published data on isotopes lighter than ^{204}Rn [6]. Some γ-ray spectroscopy of excited states in light radon and polonium isotopes has been performed recently [7,8]. The isotopes studied so far do not encroach upon the predicted region of deformation. No sudden changes in 2_1^+ energy have been observed and the 2_1^+ energy never assumes a low enough value to be associated with a strongly deformed system. In summary, there is no clear experimental evidence with which to corroborate the predictions of theoretical calculations made over the past thirty years.

The isotope ^{202}Rn is predicted to be the last neutron-deficient species with a near-spherical shape in the chain of radon isotopes; isotopes lighter than ^{202}Rn, ^{206}Ra, and ^{208}Th are expected to exhibit permanently deformed ground-state shapes [5]. The onset of deformation between ^{202}Rn and ^{200}Rn is predicted to be sudden, the calculated deformation parameters being $\epsilon_2=-0.1$ and $\epsilon_2=-0.2$, respectively [5]. This onset should be reflected in changes in the low-lying nuclear levels with a fall in the first 2^+ excitation energy and the development of a ground-state rotational band. This paper presents the experimental measurements concerning γ-ray transitions between excited states in ^{200}Rn, an isotope with a large predicted deformation parameter, $|\epsilon_2|\sim 0.2$.

II. EXPERIMENTAL DETAILS

The results presented here concern the use of the ^{176}Hf (^{28}Si,$4n$) reaction to populate excited states in ^{200}Rn. The production cross sections for heavy residues from heavy-ion fusion evaporation reactions are severely limited by the high probability for fission decay of the compound system in comparison to the probability for evaporation of light particles. The estimated production cross section of ^{200}Rn in the current reaction was estimated to be 5 μb (discussed in detail below), whilst the total fusion cross section, as predicted in a Bass model [9] calculation, is 196 mb at the beam energy used. The study of γ-ray transitions between excited states in the evaporation residues is therefore hampered by a large background of radiation from the decay of fission fragments, in addition to a large flux of γ rays associated with Coulomb excitation of the target nuclei.

In the present study an in-flight mass spectrometer is used to identify the species of interest. In the case of heavy, slow moving residues the techniques employing prompt γ-ray coincidences with recoiling ions can encounter difficulties. Whilst in general primary beam rejection can be achieved at the level of about 1 in 10^{12} particles, the production cross

*Present address: Bechtel-Nevada, W.A.M.O., P.O. Box 380, Suitland, MD 20752-0380.

sections may be so low that it becomes difficult to disentangle heavy recoiling species of interest from scattered beam particles. Such scattered beam may have true prompt γ-ray coincidences associated with Coulomb excitation leading to backgrounds of comparable strength to the radiation of interest. In addition, the energy-loss characteristics of high-Z recoiling ions alone are insufficient to make unambiguous measurements of the atomic number. Unique isotopic identification becomes difficult without the use of more selective techniques.

In the present study prompt γ rays emitted at the target position were tagged by the subsequent radioactive decay of the emitting ion after it has reached the focal plane of the mass separator. This technique was first used in a radiative fusion study of ^{180}Hg [10] and has recently been applied to large arrays of γ-ray detectors [11]. The γ rays are observed in coincidence with recoiling ions, which after transportation through the separator to a suitable detector, decay by emitting radioactivity with characteristics corresponding to the isotope of interest. Employing this technique circumvents the two problems discussed above. Beam particles are stable and do not undergo radioactive decay. Isotopic identification is made on the basis of the characteristics of the radioactive decay process, in addition to m/q measurement. In the present case, all the residues produced in the reaction decay by the emission of α particles from the ground or isomeric states. Measurements of the α-particle energy and the half-life of the decay, along with m/q, overdefine the nature of the isotope produced giving an unambiguous assignment of the neutron and proton numbers.

Beams of $^{28}Si^{7+}$ ions at energies of 142 MeV, delivered by the Argonne Tandem-Linac Accelerator System, were used to bombard both self-supporting and carbon-backed targets of hafnium oxide of thicknesses 350 and 200 μg cm^{-2}, respectively. The carbon backings used were of thickness 40 μg cm^{-2}. Ions recoiling from the reactions of ^{28}Si beam particles with carbon and oxygen nuclei in these targets do not have the correct kinematic characteristics to allow efficient transportation to the focal plane of the mass separator used, the details of which are described below. In addition, these recoils do not decay by α radioactivity. These reactions are therefore not significant sources of contamination in this experiment. The hafnium oxide used to prepare the target was isotopically enriched to a level $>70\%$ in ^{176}Hf; other constituent isotopes have atomic mass numbers greater than 176. Reactions on these contaminant hafnium isotopes lead to the production of radon isotopes heavier than ^{200}Rn by $4n$ reactions, as apparent in α-particle energy spectra discussed below. Filtering on the α-decay properties is, however, selective enough to exclude them from the final data on ^{200}Rn.

Prompt electromagnetic radiation emitted at the reaction site was detected in the AYEBALL (Argonne-Yale-European Collaboration) array. This consisted of 19 Compton-suppressed γ-ray detectors arranged in four rings around the beam direction, surrounding the target position. This array was made up of the following hyperpure germanium detectors: eight 70%-efficient crystals, five at 151° and three at 129°, nine crystals with efficiencies between 25 and 35 %, four at 97° and five at 79°, and two low-energy photon spectrometers (planar germanium crystals) at angles of 129° and 97°. Angles are quoted with respect to the beam direction and efficiencies are quoted relative to the NaI standard. The absolute photopeak efficiency of the coaxial detectors in the array was measured to be 0.91(8)% at 1408 keV, using a calibrated ^{152}Eu source.

Ions recoiling from the target position were separated from primary beam particles and analyzed in terms of their m/q ratio using the fragment mass analyzer (FMA) [12]. This device is an in-flight recoil mass separator and was adjusted to give optimum transmission for ions of mass 200, kinetic energy 18.2 MeV, and average charge state 14.5^+. Such conditions allowed the transmission of two ionic charge states, 14^+ and 15^+, to the focal plane of the instrument. A 20 μg cm^{-2} thick carbon foil was placed 10 cm downstream of the target position to restore the equilibrium charge state of any ions undergoing internal conversion after leaving the target. Transmitted ions were detected at the focal plane of the FMA using a gas-filled parallel-plate (gridded anode) avalanche counter (PPAC). This provided signals corresponding to the horizontal and vertical positions of the ion trajectories as they crossed the focal plane, in addition to a signal corresponding to the energy lost by the ions as they passed through the gas in the detector. Ions were transported by the FMA to horizontal positions along the focal plane determined by their m/q ratio, thus allowing mass identification to be made.

The trajectories of all ions passing through the focal plane were brought to an approximate focus at a distance of 40 cm behind the nominal focal plane of the device. Recoiling ions were implanted into a double-sided strip detector placed at this approximate focus. Subsequent radioactive decay of the implanted ions was observed using signals from the strip detector. The strip detector was not sufficiently large to encompass the entire area of the approximate focus and there is a loss of ions which do not hit the strip detector. Comparison of on-line rates indicated that approximately 40% of ions passing through the focal plane were implanted into the strip detector. Irradiation of the strip detector was found to be approximately uniform. The strip detector had a thickness of 60 μm and an active area of 4×4 cm^2 which was divided into strips oriented orthogonally on each side, forming individual detector elements. There were 40 strips per side, effectively dividing the detector area into 1600 ''pixels.'' Events occurring at a particular position on the detector could be isolated and associated with the correlated implantation and subsequent decays of the same ion as discussed in detail below. The energy and time of flight of ions between the PPAC and the strip detector were recorded and used to assist the removal of secondary scattered beam particles in the off-line sorting of the data.

Five nonexclusive logical event triggers were defined using hardware electronics processing. These were implantation, decay, recoil-γ, $\gamma\gamma$, and monitor event triggers and are discussed in detail below.

The strip detector was involved in two of these triggers: implantation and decay events. An implantation trigger required the coincidence between a signal from the PPAC and a signal from the strip detector. A decay trigger required a signal in the strip detector, accompanied by the absence of a signal in the PPAC. The analog energy signals associated with each of these triggers were sent to two different banks

of spectroscopy amplifiers with gains appropriate to the different energy ranges of recoiling ions and decay α particles. Signals from these two banks of amplifiers are referred to later as implantation energy and decay energy.

A recoil-γ trigger was defined by the coincident detection of one or more prompt γ rays in the germanium array around the target and the measurement of an ion passing through the PPAC at the focal plane. These three triggers were nonexclusive in the sense that an event involving the detection of a γ ray at the target position, associated with a recoiling ion which was transmitted through the focal plane and implanted into the strip detector, corresponds to both a recoil-γ and implantation event. This type of event is of interest when tagging γ rays with radioactive decay α particles, and experimental parameters associated with the array, PPAC, and strip detector were recorded together as a single event.

The remaining two logical triggers were recognized by the data acquisition system for diagnostic purposes. Events involving the coincident firing of two or more germanium detectors in the array ($\gamma\gamma$ events) were recorded. This trigger was prescaled by a factor of 10 and the associated events were used in on-line monitoring of the detectors in the array. Prescaled triggers from a silicon detector mounted in the FMA target chamber were used to monitor the state of the target during the experiment.

A 48-bit scaler ran continuously at a rate of 10^6 Hz throughout the duration of the experiment. This scaler was interrogated every time a trigger of any sort was received by the data acquisition system. Its value was recorded along with the other experimental parameters of the event, in order to label each event with the time, relative to the beginning of the experiment, at which it occurred. This time label allows the data to be played back in sequential order during off-line sorting to build up temporal correlations between the events occurring at each ''pixel'' in the strip detector.

Data was collected for approximately 79 hours at an average beam current of 7 pnA, giving an average raw rate of a few Hz in the strip detector. The beam current used was limited by the rate in the germanium detectors, which was typically 2–3 kHz Compton-suppressed rate per detector.

III. DATA REDUCTION AND ANALYSIS

The initial procedures in off-line sorting of the data concerned gain-matching of various detector elements and determining appropriate conditions to be imposed on the data. In order to calibrate the germanium detectors, singles spectra were collected from ^{152}Eu, ^{182}Ta, ^{243}Am, and ^{56}Co sources, giving good coverage of the γ-ray energy range of interest. These spectra were used to obtain gain-matching coefficients and to perform a relative efficiency calibration for the seventeen coaxial germanium detectors in singles mode. A calculated value of $\beta = v/c = 0.014$, for particles of atomic mass 200 recoiling at 0°, was used to apply a Doppler-shift energy correction to the in-beam γ-ray data. This correction to the γ-ray energies was small since the velocity of the recoiling ions was relatively low. The low recoil velocity, combined with the use of the FMA, which restricts angles of recoiling ions $\pm 3°$ to the beam direction, leads to low Doppler broadening effects on the widths of γ-ray peaks.

The α-particle energy signals for decay events from different strips in the strip detector were gain matched using strong α-particle groups in the reaction data, avoiding the problems encountered when using an external calibration source. An α-particle energy resolution of ~ 28 keV full width at half maximum was obtained in a single spectrum produced by adding signals from all strips. This was sufficient to resolve α particles associated with the decay of radon isotopes from other groups in the spectrum as illustrated below.

In order to produce as clean a data set as possible for implantation-decay correlation analysis, implantation events were filtered to reduce the number of events caused by scattered beam hitting the strip detector. A polygonal software window was placed around the recoil-ion group in a two-dimensional spectrum of implantation energy versus the time of flight between the PPAC and strip detector.

The decay events were also filtered in order to remove events involving charge sharing between strips and misidentified implantation events. Events corresponding to the sharing of charge between individual strips on the strip detector were removed by placing a polygonal software window around the diagonal group in a two-dimensional spectrum of decay energy measured in the front strip versus the decay energy measured in the back strip for each decay event. Of all decay events, 11% were excluded by this procedure.

Initial decay energy spectra indicated a small number of events corresponding to an unphysically large decay energy, in excess of 7 MeV. As a precaution during the experiment, the energy-loss signal in the PPAC was recorded for *any* event associated with the strip detector. True decay events should obviously be associated with zero energy loss in the PPAC. It was found that 3% of all decay events were recorded with a nonzero energy-loss signal. These events corresponded to failures in the hardware identification of implantation events and were excluded by suitable filtering of the energy-loss signal for decay events.

Correlation analysis was performed to identify implantation-decay sequences at any particular position on the strip detector and to distinguish subsequent decays by generation. For isotopes produced in this reaction, only radon isotopes are expected to show strong first- and second-generation α decays [13]. Other species, such as polonium and astatine nuclei are expected to show only a first-generation α decay, since the daughter nuclei are known to undergo β decay. The thickness of the strip detector is such that it is relatively insensitive to radioactive decay β particles.

Several problems arise in establishing correlated implantation-decay sequences. Difficulties in interpretation arise if, at the same position, two implantations occur within a short time interval, or if an implantation closely follows a decay event. In such cases, it is not clear with which implantation subsequent decays should be associated. Such circumstances are excluded from analysis on the basis of a time-interval test. To be acceptable, an implantation must occur at least five minutes after any previous activity was recorded at that position. If this criterion is not satisfied, the position is ignored until a period of inactivity lasting five minutes occurs, after which the position is free for further implantation. Any activity at a certain position is therefore deemed to have ended five minutes after the last recorded event at that posi-

tion. Since the isotopes of interest have half-lives shorter than a minute, a five-minute time interval should allow most of the decays to have occurred before the position is declared clean again. The size of this time interval was chosen as it resulted in the lowest background in the α-energy correlation plots discussed below, without significant losses in the true correlation peaks.

During the off-line analysis, the following information was extracted and the appropriate two-dimensional spectra were incremented: (i) first- and second-generation α-particle energies for correlated decay sequences at any particular position on the strip detector following the implantation of a recoiling ion, (ii) m/q ratios of ions implanted into the strip detector and the α-particle energy associated with their subsequent decays for all first-generation correlations and, separately, those with a further second-generation correlation, (iii) time intervals between the implantation of ions and their subsequent α decay for the various first-generation α-particle groups, (iv) time intervals between the first- and second-generation decays for the various second-generation α-particle groups, (v) first-generation α-particle energies correlated with the γ rays emitted by the subsequently implanted ions at the target position. The information for point (v) was obtained separately for coaxial and planar germanium detectors. In both cases, random events were subtracted using information obtained from a measurement of the time of flight through the FMA. This timing information was measured using a time-to-amplitude converter triggered by the arrival of an ion at the focal plane and the detection of the γ ray. The time intervals discussed in (iii) and (iv) were, however, derived from the differences in the 48-bit scaler time stamp between consecutive events.

IV. RESULTS

A. Identification of α particle groups

The identification of α-particle groups was performed on the basis of implantation-decay sequences, by measurement of α-particle energies, half-lives, and m/q ratios of the decaying ion. All three measurements were combined to produce a self-consistent identification of the isotopes produced. The α-particle energies and m/q ratios were calibrated internally using strong lines in the spectra as discussed in detail below. The half-lives were measured using time intervals measured using the MHz scaler.

A two-dimensional spectrum of the first-generation against second-generation α-particle energies is shown in Fig. 1, for correlated implantation-α-α sequences extracted from the data. As previously mentioned, only radon isotopes are expected to exhibit strong second-generation α-decay, and the seven strong peaks in Fig. 1 are therefore identified with Rn$\rightarrow$Po$\rightarrow$Pb decay sequences for parent isotopes with $A=200$, 201, 201^m, 202, 203, 203^m, 204. The results of a two-dimensional analysis of the positions of the correlation peaks are presented in Table I. Centroids of the correlation peaks were measured by placing a two-dimensional polygonal window around the correlation peak and projecting the contents onto each axis. The spectrum was calibrated internally using the known energies of the α particles. A comparison of the observed energies with the previous results, as shown in Table I, indicates the consistency of the isotopic

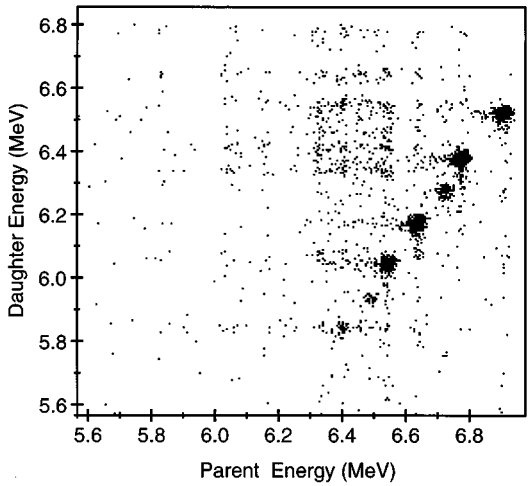

FIG. 1. A two-dimensional matrix showing the correlation between energies of first- and second-generation α decays following the reaction of ^{28}Si on ^{176}Hf. The contour level in this plot corresponds to one count per channel.

identifications made. The errors quoted in Table I for the observed energies are purely statistical. Since the α decay occurs within the strip detector, the energy measured is, in principle, higher than the nominal energy of the emitted α particle, since the recoiling daughter nucleus also deposits some energy in the detector. A systematic error, estimated for the species observed to be at most 5 keV, is introduced due to the variation of energy deposited by different recoiling daughter nuclei.

In addition to the strong correlations, a low-level pattern is seen in the spectrum which is reflection symmetric along the diagonal. This pattern is at the level of one count per channel, whilst the true correlation peaks correspond to several hundred counts per channel, and in many cases the correlations indicated in this pattern are unphysical, with second-generation α-particle energies being greater than the first. Adjustments to the time-interval test described above alter the strength of this pattern without major changes in the strength of the true correlations. This suggests that the pattern arises from residual bad correlations of the kinds discussed above.

Fine structure in α decay has recently been reported in several of the radon isotopes produced [14]. In view of the limited statistics in the present experiment, the background pattern of bad correlations in the region of the fine structure and the small branching ratios involved ($\sim 10^{-4}$), such effects are not expected to be observed here.

The masses of recoiling ions were identified using measured m/q ratios. Figure 2(a) and 2(b) illustrate this technique and show two-dimensional spectra of position along the focal plane of ion trajectories against the α-particle energy of their subsequent first-generation decay. Each α-particle energy is clearly associated with ions of a particular m/q ratio and the two different charge-state groups are clearly visible. The separation of the two charge states, and the adjacent mass groups within each one, are consistent with the expected FMA dispersion. Figure 2(b) shows a spectrum incremented only for events associated with a second generation decay and clearly identifies the seven radon

TABLE I. Measured characteristics of correlated α decay sequences involving first- and second-generation decays. Correlated first- and second-generation α groups carry the same alphabetical label. Previously measured quantities shown are taken from Ref. [27], Ref. [18], and Ref. [13]. Errors quoted on observed energies and measured half-lives are purely statistical. Contributions of systematic error to the measured energies are discussed in the text.

Parent isotope	Mass from m/q	Measured α energy (MeV)	Measured half-life (sec)	Previous α energy (MeV)	Previous half-life (sec)
(a) ^{200}Rn	200.1(3)	6.901(2)	0.96(3)	6.902(3) [a]	1.06(2) [b]
(b) ^{201m}Rn	201.2(5)	6.773(2)	3.8(1)	6.772(3) [a]	3.8(4) [c]
(c) ^{201}Rn	201.1(3)	6.725(2)	7.1.(8)	6.724(3) [a]	7.0(4) [c]
(d) ^{202}Rn	202.1(3)	6.641(1)	10.3(4)	6.641(3) [a]	9.85(20) [c]
(e) ^{203m}Rn	203.0(5)	6.551(1)	26.7(5)	6.549(3) [a]	28(2) [c]
(f) ^{203}Rn	203.2(2)	6.499(2)	42(3)	6.499(3) [a]	45(3) [c]
(g) ^{204}Rn	203.9(6)	6.420(2)	70(11)	6.419(3) [a]	74.4(18) [c]

Daughter isotope	Measured α energy (MeV)	Measured half-life (sec)	Previous α energy (MeV)	Previous half-life (sec)
(a) ^{196}Po	6.518(1)	6.8(3)	6.521(5) [a]	5.8(2) [a]
(b) ^{197m}Po	6.380(1)	32(2)	6.385(3) [c]	26(2) [c]
(c) ^{197}Po	6.281(2)	84(16)	6.282(4) [c]	56(3) [c]
(d) ^{198}Po	6.182(1)	113(7)	6.180(4) [a]	105(3) [a]
(e) ^{199m}Po	6.059(1)	260(31)	6.059(3) [c]	252(6) [c]
(f) ^{199}Po	5.953(2)	275^{+36}_{-27}	5.952(2) [c]	312(6) [c]
(g) ^{200}Po	5.862(2)	714^{+99}_{-68}	5.863(2) [c]	690(6) [c]

[a]Reference [27].
[b]Reference [18].
[c]Reference [13].

α-decay groups allowing a calibration of the focal plane in terms of m/q. The masses thus obtained are summarized in Tables I and II. A mass resolution of 1 in 170 was obtained, and, although different masses are not properly resolved in a one-dimensional m/q spectrum, two-dimensional gating techniques applied to the spectra shown in Fig. 2 allowed identification of different mass groups.

In order to isolate sequences with a single α decay, the radon intensities in the two spectra in Fig. 2 were normalized and the spectra subtracted. The projection of the resulting matrix on the α-particle energy axis is shown in Fig. 3, in comparison with α-particle energy spectra associated with other subsets of the data. Figure 3(d) contains only parent isotopes whose decay sequence involves a single α emission as the first step. Analysis confirms that the α groups in this spectrum arise from Po$\rightarrow$Pb and At$\rightarrow$Bi decays associated with masses $A=196$, 197, 197^m, 198, 199^m, 200, and $A=199$, 200, 200^m, 201, 202, 203, respectively. Measurements of α-particle energy, performed by applying two-dimensional gating techniques to the spectrum shown in Fig. 2(a) and using a calibration derived from the identification of α groups from the correlation analysis, are summarized in Table II and show good agreement with previous results.

In all cases, the presence of isotopes heavier than those expected by the nominal target isotope, ^{176}Hf, was obvious. These arise from reactions on heavier hafnium contaminants in the target, those with atomic mass numbers between 177 and 180. The residues observed are predominantly produced via $4n$, $p4n$, and $\alpha 4n$ evaporation channels, consistent with a beam energy of 142 MeV. The yields of evaporation residues associated with charged particle emission are roughly comparable to those produced in pure neutron evaporation. It has been observed that charged particle emission becomes progressively more important for isotopes further away from stability in this region; a compound system of ^{208}Rn shows very little charged-particle emission [7], whereas compound systems ^{209}Fr [15] and ^{210}Ra [16] are dominated by the evaporation of charged particles. The relative yields observed here for a compound system of ^{204}Rn appear to follow this qualitative trend. This effect is associated with fission competition and the increased fissility for systems with higher atomic number or neutron deficiency. Due to the presence of a Coulomb barrier, charged particles are emitted from a compound system with a higher average energy than neutrons, and are therefore more effective at cooling the system. Efficient cooling of the compound nucleus increases its chance of survival as fission competition is reduced by lowering compound system excitation energy. For systems of high fissility, the residues which are associated with charged-particle emission have the best chance of surviving, especially when the charged-particle is evaporated as the first step in the deexcitation. As fission competition increases with increasing atomic number or neutron deficiency, the charged-particle evaporation residues form an increasingly large proportion of the nuclei surviving fission, consistent with experimental observation.

The half-lives of the different isotopes produced were measured, where possible, by fitting exponentials to the distribution of measured time intervals between consecutive events in the decay sequences. Maximum likelihood estimates were used in the case of ^{199,200}Po, where low statistics prevented exponential fitting for events involving second-

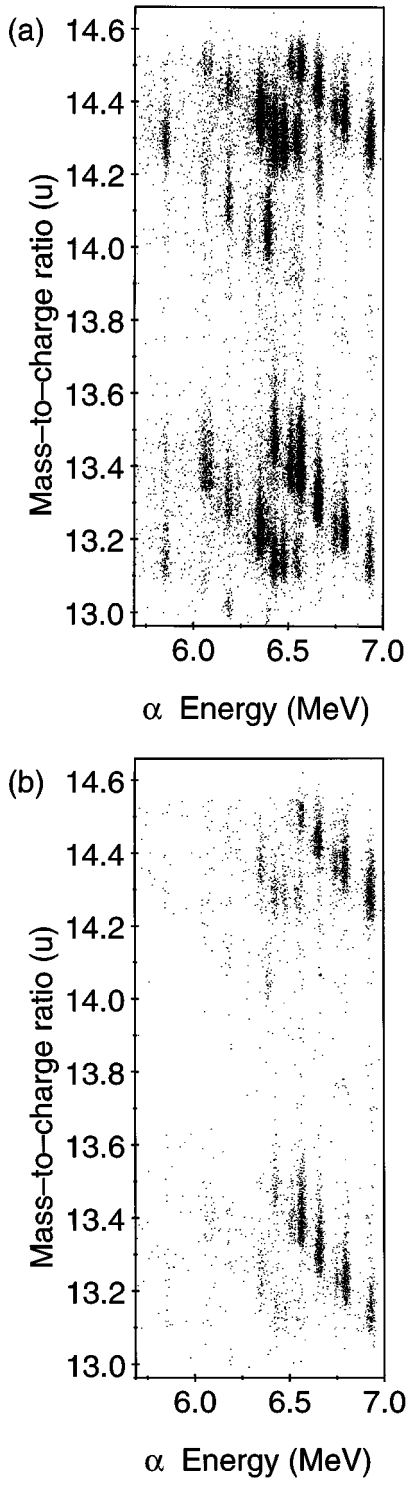

FIG. 2. A two-dimensional matrix showing the correlation between the m/q ratio of ions crossing the focal plane of the FMA and the energy of its subsequent α decay for (a) all decay sequences and (b) decay sequences involving first- and second-generation α decays. The contour level in this plot corresponds to one count per channel.

generation decays (Tables I). Half lives for the first-generation decays were measured using implantation-decay events, whereas those for second-generation decays were measured using implantation-decay-decay events. In cases where α-particle groups are not resolved in the energy spectrum, software polygonal windows were placed around the α-particle group of interest in the spectra shown in Fig. 2. Time intervals for events within the window were incremented in order to provide isolation of events associated with particular isotopes.

As an example of the quality of these data, the distribution of time intervals between implantation and decay for several isotopes are shown in Fig. 4, along with the fitted decay curves. The extracted half-lives show good agreement with previous results, as shown in Tables I and II. Three measured half-lives differ with statistical significance from previous results. The half-life of ^{197m}Po derived from events involving second-generation decays is longer than that measured previously. However, the same result derived from implantation-decay events is comparable to published data. The measured half-life of ^{200m}At appears significantly longer than that measured previously using a He-jet system [17]. For ^{200}Rn, the fit yields a half-life of 0.96(3) seconds which compares with the previously adopted value of 1.06(2) seconds [18]. Despite a significant statistical difference, no other isotopes are expected to be produced with half-lives of this magnitude and the measurement still provides reasonable identification of the ^{200}Rn group. Half-lives were not obtained for the ^{202,203}At isotopes. These nuclei were produced at very low yield and groups were contaminated by events from short-lived isotopes of the same mass, with nominally higher energy α particles. Contaminating events corresponded to cases where the α particle escaped from the strip detector without depositing its full energy.

B. Decay-tagged γ-ray data

After establishing the isotopic identity of the α groups produced in the reaction, spectra were generated of γ-ray energies, emitted by ions at the target position, which subsequently α decay with characteristics associated with particular isotopes. This provides unambiguous identification of the nuclide associated with particular γ-ray transitions. Time-random subtracted γ-ray spectra gated by α-decay consistent with ^{200,202}Rn assignments are shown in Fig. 5. Each spectrum clearly shows γ-ray transitions associated with each isotope as peaks with widths consistent with the expected γ-ray resolution. Energies and relative intensities of transitions are summarized in Table III.

Comparison of ^{200}Rn and ^{202}Rn spectra indicate the presence of a $\sim$504 keV transition in both isotopes. Whilst the measured energies are the same [504.3(2) and 504.1(3) keV, respectively, for ^{200}Rn and ^{202}Rn], the uniqueness of the isotopic selection procedure and the lack of any further degenerate γ-ray transitions, suggest that the two spectra are not cross contaminated. The transition energies and intensities measured for ^{202}Rn are in good agreement with a previous recoil-γ experiment [7], confirming those results with better isotopic identification. This consistency is indicative of the reliability of the experimental and analytical techniques employed.

The spectrum of ^{200}Rn is characterized by two transitions at energies of 432.9(2) and 504.3(2) keV. The 432.9-keV transition, being the strongest in the spectrum, is assumed to be the lowest lying in ^{200}Rn, the $2_1^+ \rightarrow 0^+$ transition. This assumption was tested by calculating the number of events

TABLE II. Measured characteristics of α decay sequences involving a single α decay. Previous data is taken from Ref. [13], apart from those marked with a superscript ''a'' taken from Ref. [27]. Other labels are used as in Table I. The α-particle energies were measured using a calibration derived from Table I and quoted errors are purely statistical. Contributions of systematic error to the measured energies are discussed in the text. The asterisk indicates that the yields were too low to allow measurement of the particular quantities, see text for details.

Parent isotope	Mass from m/q	Measured α energy (MeV)	Measured half-life (sec)	Previous α energy (MeV)	Previous half-life (sec)
^{199}At	199.3(8)	6.639(1)	8.5(10)	6.643(3)	7.0(1)
^{200m}At	200.1(3)	6.528(1)	6.3(5)	6.536(4)	4.3(3)
^{200}At	200.2(2)	6.461(1)	44(2)	6.465(2)	43(2)
^{200}At	200.2(2)	6.414(1)	47(3)	6.412(2)	43(2)
^{201}At	201.1(2)	6.342(1)	83(2)	6.344(3)	89(3)
^{202}At	*	6.229(3)	*	6.228(2)	181.2(3)
^{202}At	*	6.133(3)	*	6.135(2)	181.2(3)
^{203}At	202.9(5)	6.088(2)	*	6.088(1)	442(12)
^{197m}Po	196.9(5)	6.381(1)	29(2)	6.385(3)	26(2)
^{197}Po	196.9(12)	6.283(2)	87(18)	6.282(4)	56(3)
^{198}Po	198.0(11)	6.182(1)	110(9)	6.180(4) [a]	105(3) [a]
^{199m}Po	199.4(16)	6.059(2)	224(45)	6.059(3)	252(6)
^{200}Po	200.2(5)	5.863(2)	575(95)	5.863(2)	690(6)

[a]Data from Ref. [27].

expected, after considering efficiency and internal conversion, if the lowest-lying transition had an equal intensity to the observed 432.9 keV transition but lay at a lower transition energy. There is no evidence in the measured spectrum for such a transition lying in the energy range 80 to 400 keV at this level. Since there is no physical expectation that the lowest-lying transition should have an energy below this range, the 432.9-keV transition is taken as lowest, whilst the 504-keV γ ray is assumed to correspond to the $4_1^+ \rightarrow 2_1^+$ transition.

Using the intensity of the 432.9-keV transition, the production cross section for ^{200}Rn was estimated to be approximately 5 μb. This estimate includes several efficiency factors. The transmission of recoiling ions from the target position to the focal plane is dominated by two factors. These arise from the restrictions imposed by the FMA on the charge state and angular distributions of the recoiling ions. Two charge states were transported to the focal plane and, using the semiempirical relationships discussed in Ref. [19], this contributes a factor of 30%. The acceptance of ions into the FMA was estimated to be 46%, using a multiple-scattering angular distribution calculated using the computer code SRIM [20]. A total efficiency of 14% was therefore used as an estimate of the transmission efficiency through the FMA. As discussed above, approximately 40% of all ions crossing the focal plane are implanted into the strip detector. Comparison of the number of recoil-decay correlated events with the number of full second generation correlations indicates that the efficiency of measuring an α particle which deposits its full energy into the strip detector is approxi-

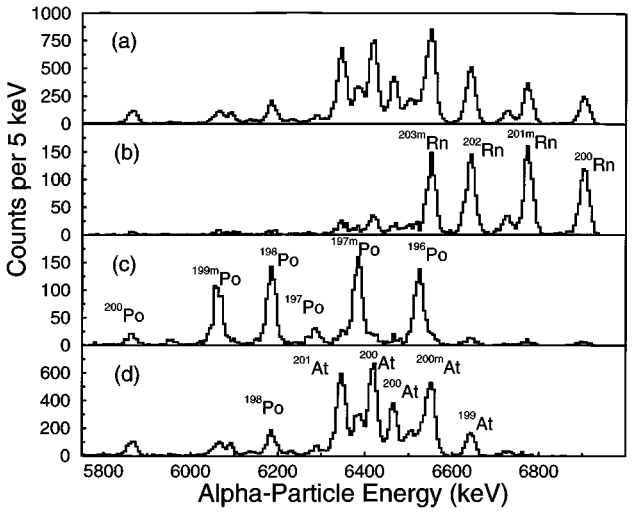

FIG. 3. Energy spectra of α particles associated with (a) any decay event in the strip detector, (b) first-generation decays for decay sequences involving first- and second-generation α decays, (c) second-generation decays for decay sequences involving first- and second-generation α decays, and (d) decays for sequences involving a single α decay, see text for details. Strong α groups are labeled with the decaying isotope.

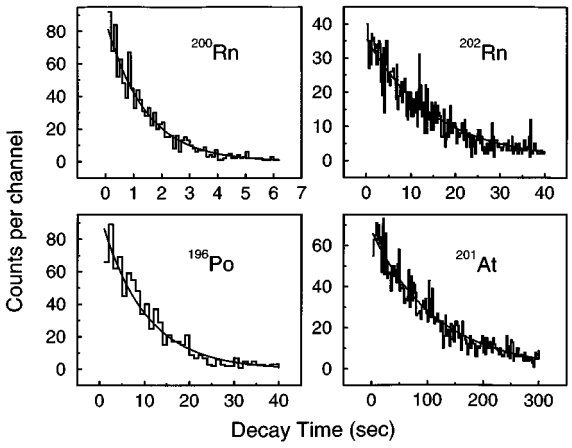

FIG. 4. The distribution of time intervals between the implantation and decay of ^{200}Rn, ^{202}Rn, ^{196}Po, and ^{201}At ions in the strip detector with the fitted decay curve.

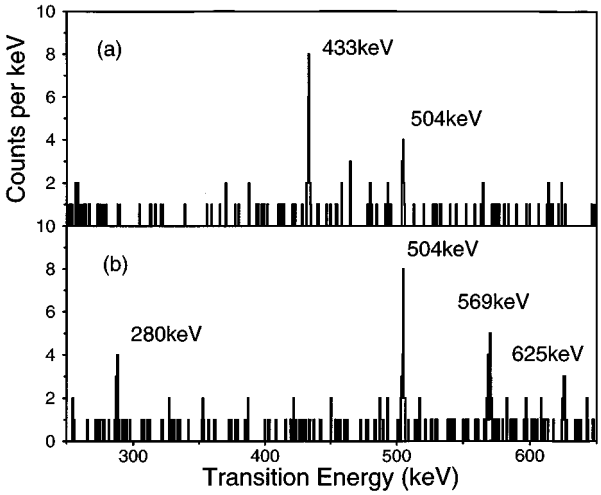

FIG. 5. Energy spectra of prompt γ rays emitted at the target position by ions which subsequently α decay in the strip detector with characteristics associated with (a) ^{200}Rn and (b) ^{202}Rn.

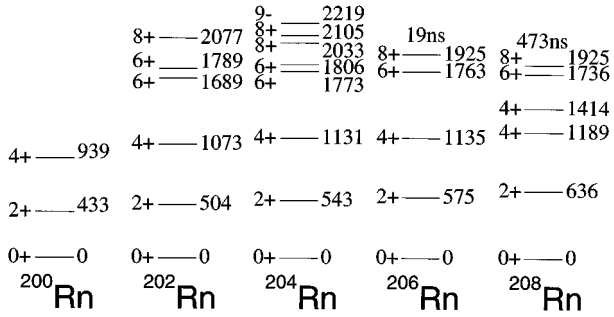

FIG. 6. Low-lying level schemes for the neutron-deficient radon isotopes. The level schemes for ^{202,204}Rn are those derived from present data and observed transitions are indicated by arrows. The half-lives of the 8^+ isomers in the heavier isotopes are indicated above the respective energy level.

mately 50%. Other α particles escape from the detector without depositing their full energy. This is due to the small implantation depth of the recoiling ions associated with low recoil velocity. The efficiency of detecting γ rays with an energy of 432 keV was estimated to be 2%, from the measured absolute efficiency at 1.4 MeV and the measured relative efficiency. The value of the production cross section must be viewed as an estimate due to the large uncertainties in each of these efficiencies and in the target thickness and beam currents used.

V. INTERPRETATION AND CONCLUSIONS

The two transitions identified in ^{200}Rn are illustrated in Fig. 6, and compared to the low-lying level schemes of heavier radon isotopes [21–24], below the $N=126$ neutron closure. The $2_1^+ \rightarrow 0^+$ transition energy in ^{200}Rn at 432.9 keV is 70 keV lower than that of ^{202}Rn. This is consistent with the gradual fall in the excitation energy of the 2_1^+ state with increasing neutron deficiency in the radon isotopes. This smooth fall can be associated with increasing mixing of neutron configurations into the proton $h_{9/2}^4$ structures, which are responsible for the low-lying states near the shell closure, as the number of neutron degrees of freedom increases. Alternatively, the softening of the nuclear shape towards deformation by increased numbers of valence neutrons, lowers the energy of the vibrational phonon states. There is no sudden fall in the 2_1^+ excitation energy, which remains at a value inconsistent with that expected for a well-deformed system with a deformation parameter, $|\epsilon_2| \sim 0.2$. Moreover, the ratio of excitation energies of the 4_1^+ and 2_1^+ states, well known to be indicative of low-lying nuclear structure, has a value of 2.16 which is typical of an anharmonic vibrational system. A clearly defined rotational system, characterized by a $E(4_1^+)/E(2_1^+)$ ratio of 3.33, is not apparent. These simple features of the low-lying structure in ^{200}Rn therefore suggest that it does not exhibit a strong permanently deformed shape at low excitation energies. The structure of the system appears to be rather vibrational in character. The predicted onset of deformation does not occur, or is delayed until lighter isotopes.

TABLE III. Relative γ-ray intensities for (a) ^{200}Rn and (b) ^{202}Rn.

	Transition energy (keV)	Intensity
(a)	432.9(2)	100(22)
	504.3(2)	60(18)
(b)	287.6(2)	33(12)
	504.1(3)	100(23)
	569.5(3)	94(25)
	625.5(3)	53(19)

These data are consistent with recent studies of the α decay of ^{204}Ra [16,25]. These studies found no evidence for fine structure in the α decay to the daughter nucleus, ^{200}Rn, indicating that the first excited state does not lie below approximately 200 keV.

The calculations of Ref. [5] indicate that ^{200}Rn is the first neutron-deficient even-even system to have a minimum in the potential-energy surface at a deformation, $|\epsilon_2| \geq 0.2$; heavier isotopes are predicted to have minima at deformations with $|\epsilon_2| < 0.1$. The lack of experimental features consistent with these predictions might suggest the influence of factors beyond the scope of the models used so far to calculate shape. For example, a delayed onset of deformation might indicate imprecise knowledge of the exact energetic location of shape-driving single-particle orbitals within the shell correction of the calculation. However, a minimum in the potential-energy surface at a large magnitude of deformation is not a sufficient condition with which to predict a stable well-deformed ground-state shape. If the minimum is not sufficiently deep, zero-point fluctuations could sample a wide range of deformation leading to a soft transitional system. Indeed, the presence of oblate *and* prolate minima, lying close in energy in these calculations, suggests that the possibility of excursions across triaxial shapes should not be discounted. Such a region of γ-soft nuclei, similar to that in the Ba-Xe region [26], is not accounted for in theoretical calculations performed so far which are restricted to axially symmetric shapes.

In conclusion, the low-lying structure of ^{200}Rn has been investigated. The radiation from the weakly produced evapo-

ration residues were identified and distinguished from intense backgrounds arising from fission fragments and Coulomb excitation by the use of mass selection and radioactive-decay tagging. The structure of ^{200}Rn is not consistent with a stable well-deformed ground-state shape, in contrast to theoretical predictions suggesting that the lowest-lying minimum is associated with a deformation parameter $\epsilon = -0.2$.

ACKNOWLEDGMENTS

This work was supported by the UK Engineering and Physical Sciences Research Council and by the U.S. Department of Energy under Contract No. W-31-109-ENG-38. One of us (R.B.E.T.) acknowledges financial support from EPSRC.

[1] E. Marshalek, L. Person, and R.K. Sheline, Rev. Mod. Phys. **35**, 108 (1963).
[2] P. Möller and J.R. Nix, At. Nucl. Data Tables **26**, 165 (1981).
[3] P. Möller, J.R. Nix, and J. Zhang, Phys. Scr. **29**, 402 (1984).
[4] T. Lönroth, R. Bengtsson, and P. Möller, Abo Akademi University, Turku, Finland, report, 1993.
[5] P. Möller, J.R. Nix, and W.J. Swiatecki, At. Data Nucl. Data Tables **59**, 185 (1995).
[6] J. Billowes and P. Campbell, J. Phys. G **21**, 707 (1995).
[7] S.J. Freeman *et al.*, Phys. Rev. C **50**, 1754 (1994).
[8] W. Younes *et al.*, Phys. Rev. C **52**, 1723 (1995).
[9] R. Bass, Phys. Rev. Lett. **39**, 265 (1977).
[10] R.S. Simon, K.-H. Schmidt, F.P. Hessberger, S. Hlavac, M. Honusek, G. Münzenberg, H.-G. Clerc, U. Gollerthan, and W. Schwab, Z. Phys. **325**, 197 (1986).
[11] E.S. Paul *et al.*, Phys. Rev. C **51**, 78 (1995)
[12] C.N. Davids and J.D. Larson, Nucl. Instrum. Methods Phys. Res. B **40/41**, 1224 (1989).
[13] E. Browne and R.B. Firestone, in *Table of Radioactive Isotopes*, edited by V.S. Shirley (Wiley, New York 1986).
[14] N. Bijnens *et al.*, Phys. Rev. Lett. **75**, 4571 (1995).
[15] S.J. Freeman, Phys. Scr. **56**, 249 (1995).
[16] M.J. Leddy, S.J. Freeman, J.L. Durell, A.G. Smith, S.J. Warburton, D.J. Blumenthal, C.N. Davids, C.J. Lister, and H.T. Penttilä, Phys. Rev. C **51**, 1047 (1995).
[17] William Treytl and Kalevi Valli, Nucl. Phys. **97A**, 405 (1967).
[18] F. Calaprice, G.T. Ewan, R.-D. von Dincklage, B. Jonson, O.C. Jonsson and H.L. Ravn, Phys. Rev. C **30**, 1671 (1984).
[19] Hans-Dieter Betz, Rev. Mod. Phys. **44**, 465 (1972).
[20] J.F. Zeigler, computer code SRIM96 (unpublished).
[21] D. Horn, C. Baktash, and C.J. Lister, Phys. Rev. C **24**, 2136 (1981).
[22] B.G. Ritchie, F.T. Avignone III, H.K. Carter, R.L. Mlekodaj, and E.H. Spejewski, Phys. Rev. C **23**, 1717 (1981).
[23] A.R. Poletti, G.D. Dracoulis, C. Fahlander, and I. Morrison, Nucl. Phys. **A380**, 335 (1982).
[24] W.J. Triggs, A.R. Poletti, G.D. Dracoulis, C. Fahlander, and A.P. Byrne, Nucl. Phys. **A395**, 274 (1983).
[25] M. Leino *et al.*, Z. Phys. **355**, 157 (1996).
[26] R.F. Casten and P. von Brentano, Phys. Lett. **152B**, 22 (1985).
[27] J. Wauters, P. Dendooven, M. Huyse, G. Reusen, and P. Van Duppen, Phys. Rev. C **47**, 1447 (1993).